Nanoscale

RSC Publishing

PAPER

View Article Online
View Journal | View Issue

Cite this: *Nanoscale*, 2013, **5**, 10534

Inorganic chemistry in a nanoreactor: Au/TiO_2 nanocomposites by photolysis of a single-source precursor in miniemulsion†

Niels A. Heutz,*[a] Paolo Dolcet,[b] Alexander Birkner,[c] Maurizio Casarin,[b] Klaus Merz,[a] Stefano Gialanella[d] and Silvia Gross*[e]

An original synthetic route, based on the combination of a single-source precursor, UV-photodegradation and inverse w/o miniemulsion, is used to prepare Au nanoparticles (NPs) dispersed on titania. The source of the nanocomposite materials is the photolabile single-source precursor $AuCl_4(NH_4)_7[Ti_2(O_2)_2(cit)(Hcit)]_2 \cdot 12H_2O$, which is suspended in a w/o miniemulsion consisting of different surfactant/hydrocarbon/water formulations (surfactant: sodium dodecylsulfate (SDS) or Triton X-100) and subsequently irradiated with a UV lamp to promote its decomposition in the confined space of the droplets. Gold NPs that form at room temperature are found to be crystalline, while titanium dioxide occurs as an amorphous phase. Moreover, the average crystallite size of gold NPs ranges between 20 and 24 nm when using SDS and between 26 and 40 nm in the case of Triton X-100, after 4 and 8 hours of irradiation time, respectively. Scanning and transmission electron microscopies (SEM and TEM) are used to get information about the nanocomposite morphology and nanostructure, revealing that gold NPs are uniformly distributed on the titanium oxide surface. Furthermore, X-ray photoelectron spectroscopy (XPS) outcomes, besides confirming the formation of both metallic gold and titania, provide information about the high dispersion of Au NPs on the TiO_2 surface. In fact, the Au : Ti atomic ratio is found to be 0.45–1.5 (1 : 2–1.5 : 1), which is higher than the value determined by starting from the precursor stoichiometry (0.25). Catalytic testing in the oxidation of 2-propanol shows that decomposition of the precursor in a miniemulsion provides a nanocomposite with enhanced activity compared to the decomposition in the aqueous phase.

Received 31st July 2013
Accepted 9th August 2013

DOI: 10.1039/c3nr03977c

www.rsc.org/nanoscale

Introduction

The versatility and the wide range of possible applications in the oxidation catalysis make the nanocomposite systems M/TiO_2 (M = Au, Pd, Pt) the focus of growing interest.[1–7] The specific characteristics of these systems are ultimately associated with the weak interactions occurring at the metal–oxide interface,[8,9] which are a key factor to enhance the M/TiO_2 catalytic activity, for instance in CO and alcohol oxidation.[10–12] Au/TiO_2 has also been proven to be an effective catalyst for NO_x reduction and the water gas shift reaction.[13,14] Furthermore, this nanocomposite has also been investigated for its outstanding photocatalytic properties[2,6,15,16] as well as for the development of photoelectrochemical solar cells.[8,17] The interest devoted to Au/TiO_2 systems is also motivated by their potential use in non-linear optical devices, due to the high polarizability of gold nanoparticles and the dielectric nature of the titania matrix.

We present here an original synthetic route, based on the combined use of (i) a single-source precursor, (ii) UV-photodegradation and (iii) a miniemulsion, to prepare Au nanoparticles (NPs) dispersed on TiO_2. Droplets formed during the miniemulsification process, which was pioneered by Landfester and co-workers,[18–25] can be used as nanoreactors which maximize the co-penetration of the two components, thus allowing us to obtain the NP nucleation and growth in a confined space. This in turn enables good control of particle size, size distribution and morphology, all of them playing a crucial role in determining the important functional properties of the resulting materials.

In this paper, we successfully explored, to the best of our knowledge for the first time, the use of water-in-oil droplets produced by a miniemulsion as nanoreactors for the *in situ* UV-photodecomposition of a tailor-made single-source precursor

[a]*Lehrstuhl für Anorganische Chemie I, Fakultät für Chemie und Biochemie, Ruhr-Universität Bochum, Universitätsstr. 150, D-44801 Bochum, Germany. E-mail: niels.heutz@rub.de; Tel: +49 234 3224177*

[b]*Dipartimento di Scienze Chimiche, University of Padova, INSTM, UdR Padova, Via Marzolo, 1, I-35131, Padova, Italy*

[c]*Lehrstuhl für Physikalische Chemie I, Fakultät für Chemie und Biochemie, Ruhr-Universität Bochum, Universitätsstr. 150, D-44801 Bochum, Germany*

[d]*Dipartimento di Ingegneria Industriale, University of Trento, Via Mesiano 77, 38123 Trento, Italy*

[e]*Istituto per l'Energetica e le Interfasi, IENI-CNR and Dipartimento di Scienze Chimiche, Università degli Studi di Padova, Via Marzolo, 1, I-35131, Padova, Italy. E-mail: silvia.gross@unipd.it*

† Electronic supplementary information (ESI) available: SEM and TEM images, detailed XPS peaks, thermogravimetric analysis, XRD patterns of catalysis samples and the Raman spectrum of $AuTi_4$. See DOI: 10.1039/c3nr03977c

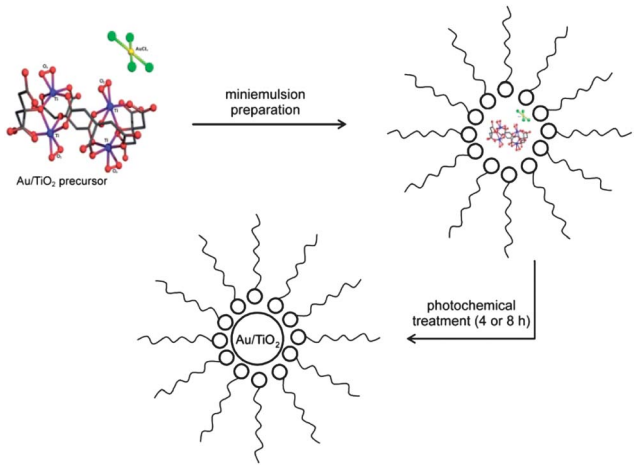

Scheme 1 Formation of Au/TiO_2 nanocomposite in miniemulsion by photolysis of $AuCl_4(NH_4)_7[Ti_2(O_2)_2(cit)(Hcit)]_2 \cdot 12H_2O$.

containing both gold and titanium to give the Au/TiO_2 nanocomposite. The synthesis strategy is depicted in Scheme 1. The cluster $AuCl_4(NH_4)_7[Ti_2(O_2)_2(Hcit)(cit)]_2 \cdot 12H_2O$ (hereafter $AuTi_4$), prepared as described elsewhere,[6] is well known for its easy photolysis under UV irradiation. $AuTi_4$ has a well-defined structure, characterized by the coordination of titanium atoms by citric acid and peroxide groups, which favour the reduction of Au(III) to metallic gold[26] and the formation of TiO_2 modifications,[27,28] respectively. The addition of an aqueous $AuTi_4$ precursor solution to different surfactants (sodium dodecylsulfate (SDS) or Triton X-100)/hydrocarbon suspensions and subsequent ultrasonication resulted in a homogeneous yellow-coloured water-in-oil miniemulsion. Once the single-source precursor was embedded into the inverse micelles, the decomposition of the photolabile precursor was triggered by UV irradiation of the suspension to achieve the formation of the Au/TiO_2 nanocomposite directly in the nanocompartments, as sketched in Scheme 1.

Results and discussion

Experiments were carried out by changing the experimental parameters (irradiation time, chemical nature of the surfactant and dispersing phase), as summarized in Table 1, to relate their variation to the final features of the obtained nanocomposites. According to the different irradiation times and surfactants used for the preparation of the Au/TiO_2 nanocomposites, they are labelled as shown in Table 1.

Table 1 Sample labelling and experimental parameters used

Sample	Irradiation time [h]	Surfactant	Miniemulsion
SDS-4	4	SDS	SDS/pentanol/heptane
SDS-8	8	SDS	SDS/pentanol/heptane
T100-4	4	Triton X-100	Triton X-100/pentanol/cyclohexane
T100-8	8	Triton X-100	Triton X-100/pentanol/cyclohexane

Preparation of Au/TiO_2-nanocomposites in miniemulsions

Preparation in miniemulsions using the non-ionic surfactant Triton X-100. To investigate the effect of the surfactant, affecting droplet stability, as well as their size and morphology, experiments on the formation of Au/TiO_2 nanocomposites from miniemulsions were first performed by using a non-ionic surfactant, Triton X-100 (see Experimental section). The obtained samples were characterized by means of X-ray diffraction (XRD), transmission electron microscopy (TEM), scanning electron microscopy (SEM), X-ray photoelectron spectroscopy (XPS), and energy dispersive X-ray spectroscopy (EDXS). The results of the XRD investigations on the T100-4 and T100-8 nanocomposites, after 4 and 8 hours of irradiation time, are shown in Fig. 1. The diffraction patterns reveal the presence of fcc crystalline gold [JCPDS 4-784], whereas, although no feature ascribable to crystalline polymorphs of titania (either rutile, anatase, or brookite) was observed in the XRD patterns, the presence of titania was evidenced by XPS and EDXS analyses described in the following sections. The single crystallite sizes of the gold NPs in the nanocomposites, as evaluated from the Scherrer equation, were determined to be 26 nm after 4 hours and 40 nm after 8 hours of irradiation time, respectively. In agreement with TEM measurements (*vide infra*), this shows that increasing the irradiation time induces a growth of the metallic gold nanoparticles. In this regard, TEM micrographs (see Fig. 2) display two features representative of the microstructure of both T100-4 and T100-8: a fine dispersion of a few nanometer sized gold particles, suspended on the titania matrix, and coarser gold particles, still in the nanometric range.

Incidentally, this distribution is evidenced also by the SEM images, recorded by using the back-scattered electrons, in order to enhance the Au NP signal and allow a better size and distribution determination (see Section 1 in the ESI†). The described microstructural and crystallographic evidence is in agreement also with the SAED pattern in which gold spots and rings, although extremely weak, are visible in association with the amorphous halo. The surface composition of the nanocomposite was analyzed by XPS, providing details on both atomic percentages and chemical state of the present species. The survey spectrum (Fig. 3, top) of the powder shows peaks referring to the elements Au, Ti, O, C, and N. Details of the

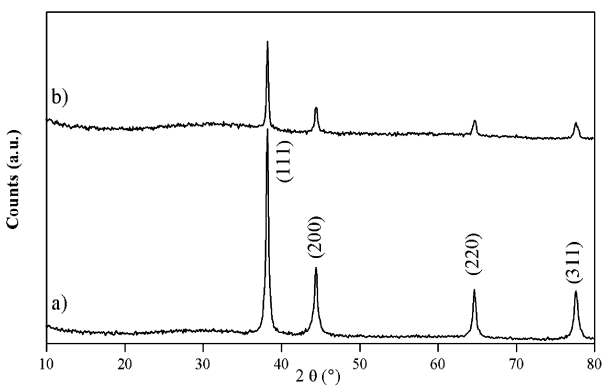

Fig. 1 XRD patterns of Au/TiO_2 nanocomposites: (a) T100-4 and (b) T100-8.

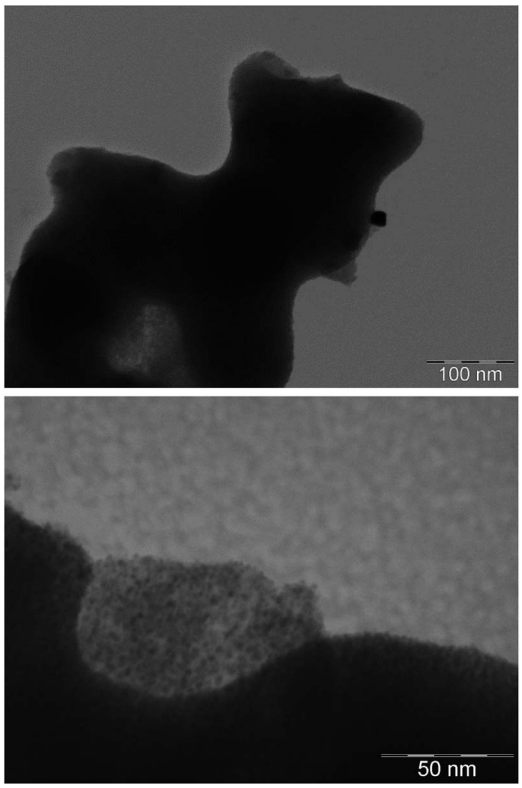

Fig. 2 TEM micrographs of the Au/TiO_2 nanocomposites: (top) T100-4 and (bottom) T100-8.

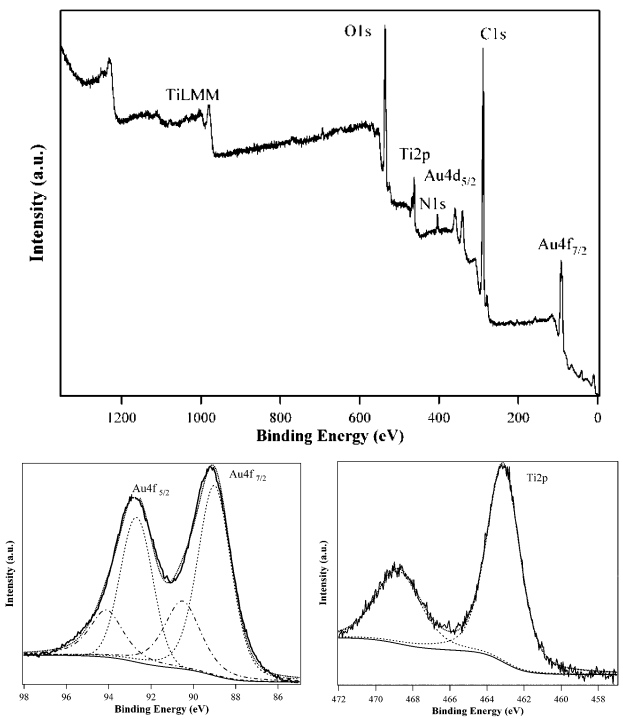

Fig. 3 XPS spectra of T100-4 (survey, Au4f, and Ti2p region).

atomic percentages and Binding Energy (BE) values of the different species are summarized in Table 2 and detailed spectra can be found in the ESI (see the ESI – Section 2†). Au4f, Ti2p, and O1s are related to the Au/TiO_2 nanocomposite, while C1s and N1s peaks indicate residues of the surfactant and precursor. As far as the chemical nature of the different species is concerned, the deconvolution of the Au4f region (Fig. 3, bottom left) shows that two different species of Au are present in the T100-4 nanocomposite. While the BE values of the doublet at 84.7 eV and 88.3 eV are in good agreement with elemental gold,[2,5,29–32] two smaller peaks are observed at energies of 85.4 eV and 89.1 eV, thus revealing the presence of Au(III) species which can be reasonably ascribed to an incomplete decomposition of the precursor. However, the contribution to the Au(III) peak area is small, thus indicating that the precursor was mostly successfully decomposed. For T100-4, the Au(0) to Au(III) ratio (referring to the peak areas) is 2.8, indicating that the degree of conversion is as high as 74%. Although T100-8 was obtained after 8 h of irradiation, the nanocomposite still displays the presence of two gold species. The peaks referring to Au(III) contribute only to a little extent to the overall peak area, showing a Au(0) to Au(III) ratio of 2.3 (Table 3). The reason why, in this second case, a longer irradiation time does not promote a higher decomposition extent of the precursor is not clear, and it is currently under investigation. It can be argued that the longer irradiation time affects the growth of the NPs (*vide infra*) but not the decomposition rate and efficiency.

Preparation in miniemulsions using the ionic surfactant SDS. In order to compare the obtained results with a different

Table 2 Elemental atomic percentages and binding energy values as determined by XPS

	BE (eV)			Atomic composition[c] (%)			
Sample	BE[a] O1s	BE[a] Ti2p	BE[b] Au4f	Ti	O	Au	C
SDS-4	529.8	459.2	84.2	2.0	21.0	3.0	74.0
	531.7	460.8	87.1				
SDS-8	529.2	461.1	84.7	2.5	21.0	2.5	74.0
	531.0	466.6	86.9				
T100-4	531.4	460.2	84.7	2.4	19.6	2.0	76.0
		465.8	85.4				
T100-8	530.2	458.6	83.9	9.4	40.0	4.2	46.4
		464.3	85.3				

[a] Values corrected for charging effects, using 284.6 eV as the carbon standard. [b] Values corrected for charging effects, using cross referencing with 458.8 eV as the titania standard. [c] Surface atomic composition determined from XPS data.

Table 3 Elemental atomic ratios and gold crystallite sizes of the Au/TiO_2 nanocomposites

Sample	T100-4	T100-8	SDS-4	SDS-8
Crystallite size[a] (nm)	26	40	26	25
Au/Ti ratio[b]	0.83	0.45	1.5	1
Au(0)/Au(III)[c]	2.8	2.3	2.2	7.3
Auger parameter α'	873.0 eV	872.9 eV	875.2 eV	873.9 eV

[a] Average particle size estimated from XRD data by using the Scherrer equation. [b] Calculated from atomic composition found by XPS. [c] Estimated from the deconvoluted peak areas of the Au4f regions.

miniemulsion system, Au/TiO_2 nanocomposites were prepared in a SDS-based miniemulsion. Samples were then prepared at irradiation times of 4 and 8 hours. XRD investigations on the obtained samples SDS-4 and SDS-8 show similar results to T100-4 and T100-8. As expected, also the Au/TiO_2 nanocomposites SDS-4 and SDS-8 consist of crystalline gold nanoparticles supported on amorphous titania. The diffraction pattern of SDS-4 in Fig. 4 confirms the presence of fcc crystalline gold [JCPDS 4-784], whereas no evidence for crystalline titania phases is observed in the XRD pattern. All this evidence mirrors the results pertaining to the nanocomposites obtained as described before. At variance with T100-4, a slightly smaller average crystallite size of about 20 nm was estimated for SDS-4. TEM analysis on the same sample substantially confirmed the picture conveyed by XRD. Gold particles appear as darker grains in Fig. 5, referring to sample SDS-4. Their size (about 100 nm), larger than the average crystallite size value provided by XRD data, indicates that they are composed of several coherently scattering domains that coalesced during the growing process. Further investigations show regions of the specimen where the presence of the above nanocrystalline gold grains is not obvious (Fig. 5) although the relevant EDXS data indicate that gold is present in these regions too. The higher magnification image shows that gold particles of about 3 nm are finely dispersed on the titania matrix (Fig. 5). Deeper insights into the morphology of the composite sample and the nanoparticle distribution were obtained by systematic SEM and TEM investigations on all synthesized materials (see the ESI– Sections 1 and 3†). XPS investigations on SDS-4 and SDS-8 give comparable results to those on T100-4 and T100-8. The survey spectra also show element specific peaks related to gold, oxygen, titanium, nitrogen, and carbon, which can be related to Au/TiO_2 and to residues of the precursor.

Detailed results of the surface composition, in particular atomic percentages and binding energy values of the different species, are summarized in Table 2 and detailed spectra are reported in the ESI.†

As for T100-4 and T100-8, the successful formation and the extent of precursor degradation were estimated from detailed XPS investigations on the gold species found in the samples. The Au : Ti atomic ratio on the surface of the powder sample

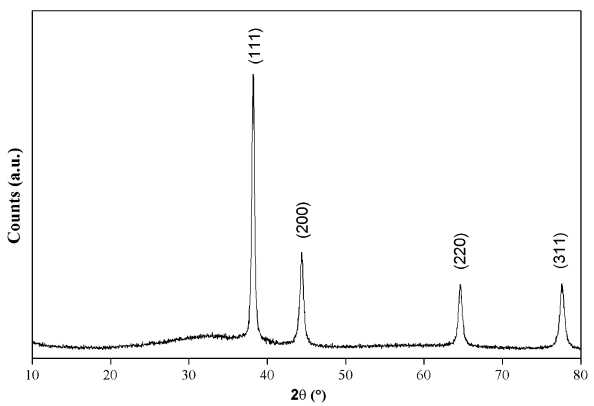

Fig. 4 XRD pattern of SDS-4.

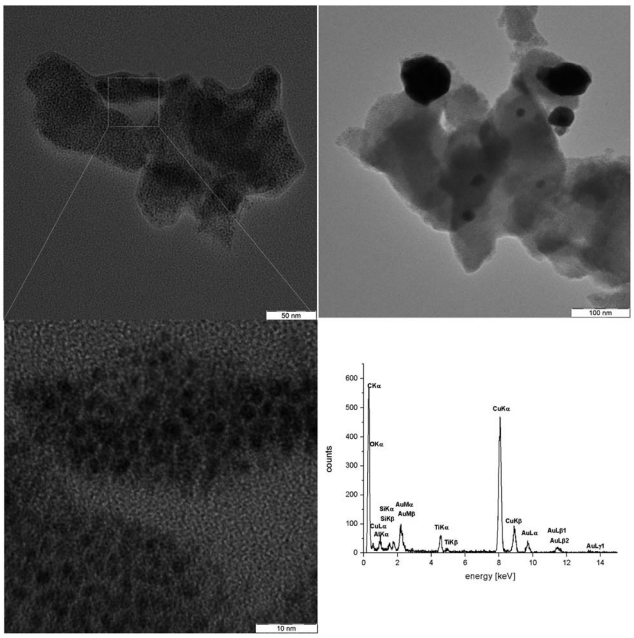

Fig. 5 TEM and EDXS of SDS-4 obtained after 4 hours.

SDS-4 is 1.5, whereas on the basis of the stoichiometry of the precursor a value of 0.25 could be expected. The enrichment of gold in the outer part of the material can likely be ascribed to the migration of gold towards the outer layers of the titania support and to the high surface sensitivity of XPS. The phenomenon of segregation of metallic nanoparticles in oxide matrices has been unanimously accepted.[5,33–36] The high amount of carbon has to be ascribed to the presence of surfactants. Actually, the deconvolution of the C1s region (see the ESI – Section 11†) revealed three components at 284.6, 285.9 and 288.4 eV. The first component is assigned to the aliphatic chains of the surfactant, the second one to –C–O–R groups, and the last one has a typical value for oxygen in carboxyl groups and can therefore be ascribed to residual citrate.

In this regard, to evaluate the effective amount of surfactant surrounding the nanoparticles, thermogravimetric analysis was carried out, revealing a weight loss, mostly due to water, to a 12% w/w extent and to the surfactant of about 17% w/w (see the ESI – Section 17†). Also the O1s region consists of two components (see the ESI – Section 12†), one at 530.1 eV, ascribed to oxygen in the titania lattice,[2,5,37] and the latter and most intense one at 531.7 eV ascribed to the oxygen atoms of the surfactants. The presence of nitrogen has to be ultimately traced back to the presence of residual ammonium groups in the single-source precursor, whereas sulphur of the sulphate group in the surfactant could not be detected. Particularly interesting is the analysis of Ti2p and Au4f regions, shown in Fig. 6. The $Ti2p_{3/2}$ feature of the Ti2p doublet is characterized by two components, the most intense one at 459.2 eV, typical of titanium dioxide,[2,37–39] whereas the latter one, at 460.8 eV, can be ascribed to the chemical environment of titanium in the precursor, thus suggesting an incomplete decomposition. This hypothesis is further strengthened also by the Au4f region deconvolution, showing two $Au4f_{7/2}$ components at 84.2 eV and 87.1 eV.

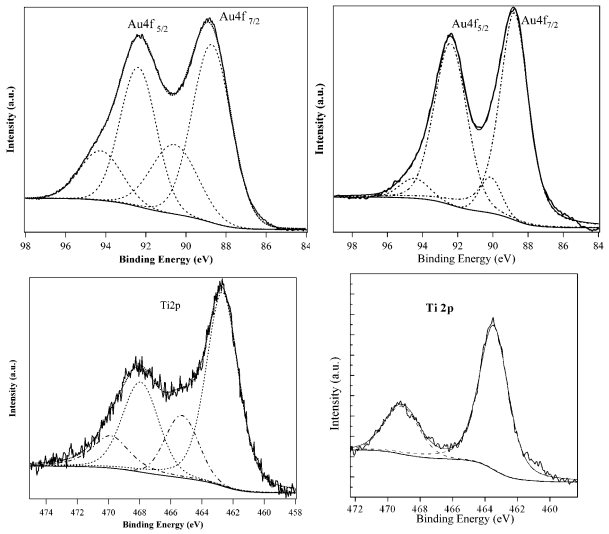

Fig. 6 XPS spectra of the Au4f (top) and Ti2p (bottom) regions of SDS-4 (left) and SDS-8 (right).

The peak at 84.2 eV corresponds to metallic gold,[2,29,30] whose presence was already evidenced by XRD analysis; the latter, at a higher energy peak (87.1 eV), was assigned to Au(III), in agreement with the above-mentioned incomplete precursor decomposition. However, it has to be pointed out that, as in the previous case, the component associated with the residual precursor has a much lower intensity than that ascribed to metallic gold on titania. As shown in Table 3, the peak area ratio of metallic gold with respect to the residual precursor line is 2.2 : 1.0, thus evidencing that the chosen route to obtain the desired compound was slightly less effective than that implying the non-ionic surfactant based droplets. In addition to the Ti2p region, the TiLMM region was also acquired to estimate the Auger parameter α' of Ti, to unambiguously determine its chemical state. The TiO_2 Auger parameter reported in the literature is 872.9 eV.[40] Detailed investigations on the interaction between TiO_2 and metals have been reported by Mejias *et al.*[41] Experimental values were, for T100 samples, in accordance with literature data. Nevertheless a α' value of 875.2 eV was calculated for SDS-4, *i.e.*, the sample with the highest Au/Ti ratio (1.5, as determined by XPS surface analysis). This finding is in very good agreement with published results,[41] which show that higher α' values are observed at a high M : TiO_2 ratio.

On the basis of XPS findings, pointing out the presence of undecomposed precursor, the irradiation time was doubled from 4 to 8 hours to trigger the complete decomposition of the Au–Ti precursor to the desired nanocomposite. The Au4f region still presents two contributions, as for SDS-4 (see Fig. 6); intense signals at 84.7 eV and 87.3 eV are in good agreement with Au4f signals of elemental gold, while the signals of lower intensity at 86.9 eV and 90.6 eV can be ascribed to the presence of Au(III) species. Compared to the Au4f region of SDS-4, though, a strong decrease of the peak intensity related to Au(III) is observed after 8 hours of irradiation in the case of SDS-8, evidencing therefore an increased precursor decomposition.

The ratio of metallic gold to residual Au(III) increased from 2.2 to 7.3, which clearly indicates an increased degradation of the precursor to form Au/TiO_2. This finding confirms the successful improvement of the precursor decomposition in the miniemulsion system by using the SDS-based miniemulsion. Compared to SDS-4 the deconvolution of the Ti2p region shows just one component. Signals at 461.1 and 466.6 eV refer to titanium dioxide. This is in agreement with our finding for O1s, where the signal at 529.2 eV can be ascribed to titanium dioxide, while the signal at 531.0 eV has to be assigned to the oxygen of the surfactant. Furthermore, in analogy with SDS-4, a higher value of the Auger parameter α' (873.9 eV) was determined for SDS-8, which is thus characterized by a gold surface enrichment; this assumption is basically confirmed also by SEM investigations (see the ESI – Section 1†). Also XRD investigations on SDS-8 revealed similar results to those on SDS-4. The diffraction pattern confirms the presence of fcc crystalline gold and no reflections ascribable to crystalline titania. The average size of the gold crystallites, estimated by using the Scherrer equation, is approximately 25 nm. In contrast to the use of a non-ionic surfactant, the miniemulsion system based on SDS seems to be more suitable to obtain smaller gold nanocrystallites or at least to limit their growth upon prolonged irradiation time.

Coherently with these indications, even TEM observations revealed a similar microstructure to that observed in sample SDS-4, as concerns in particular the coexistence of very fine and coarser gold particles. This is clearly shown by the TEM micrographs and relevant SAED patterns (see the ESI – Section 3†).

The diffraction spots, coming from the coarser particles, and the faint rings, overlapped with the amorphous halo from the titania matrix and carbon supporting film, can be both indexed to the fcc structure of metallic gold. Taken together, all these data demonstrate that the SDS-based miniemulsions are more efficient in triggering the decomposition of the precursor to yield finely dispersed gold nanoparticles on a titania matrix.

Catalytic testing – oxidation of 2-propanol

In order to investigate the influence of miniemulsions as nanoreactors on the formation of Au/TiO_2 from $AuTi_4$, the catalytic activity of the miniemulsion-prepared samples was compared to that prepared by the original route based on the decomposition of the single-source precursor in water.[6] Therefore the most promising sample SDS-8 was tested in the gaseous and liquid phase oxidation of 2-propanol as a model reaction.

Compared to the standard route, described in ref. 6 and based on the photodecomposition of $AuTi_4$ in a simple aqueous suspension, the application of miniemulsions for achieving the formation of the nanocomposite seems to be beneficial for the preparation of catalytically active Au/TiO_2. In both tests, oxidation in the gaseous phase and liquid phase, the material from the miniemulsion shows almost twice the activity (see Table 4). In the gaseous phase, an almost complete conversion and a high selectivity of 80% are observed for the sample prepared in the miniemulsion.

Table 4 Results from catalytic testing (for details see the Experimental section)

	Gaseous phase oxidation		Liquid phase oxidation
Synthetic route	Conversion	Selectivity	TOF[c] [mol $mg_{(Cat)}^{-1}$ h^{-1}]
Miniemulsion[a]	98%	80%	0.012
Solution[b]	53%	50%	0.006

[a] SDS used as a surfactant, 8 h of irradiation time. [b] Preparation as described in ref. 6. [c] Calculated for a reaction time of 2.5 hours.

In contrast, the sample prepared in water shows only 53% conversion and lower selectivity. Also the turnover frequencies (TOFs), estimated by oxidation in the liquid phase, show twice the activity for the sample from the miniemulsion. This indicates that the miniemulsion as reaction medium influences the formation and properties of Au/TiO_2 and thereby enhances the catalytic activity.

XRD investigations (see the ESI – Section 18†) on both samples show that the gold crystallite sizes prepared in a miniemulsion and aqueous phase are 29 nm and 39 nm respectively. One explanation for this finding is that gold particles easily form agglomerates[42] in the aqueous phase and therefore tend to coalesce to bigger particles under the elevated temperature employed during the pre-treatment before the catalytic testing (see the Experimental section for further details). This indicates that preparation in a miniemulsion induces the enhanced stability of the gold particles, inhibiting at the same time particle growth during thermal treatment. Furthermore, the uniform distribution of gold nanoparticles on the titania matrix could also positively affect the catalytic activity. Thereby a more active nanocomposite is obtained compared to the original preparation method in water. These results underline the advantageous properties of miniemulsions as nanoreactors for the preparation of inorganic composite materials with unusual morphologies, controlled size and enhanced functional properties.

Conclusions

In summary, we obtained nanocrystalline gold dispersed on titania by using an original route based on photolysis of a single-source precursor in a confined space. The source of the nanocomposite materials is the photolabile single-source precursor $AuCl_4(NH_4)_7[Ti_2(O_2)_2(cit)(Hcit)]_2 \cdot 12H_2O$, which was emulsified in a w/o miniemulsion consisting of sodium dodecylsulfate/heptane/water in one case and Triton X-100/cyclohexane/water in another case, and subsequently irradiated with a UV lamp to promote its decomposition into the confined space of the droplets. Gold NPs formed at room temperature were found to be crystalline, while titanium dioxide, whose presence was confirmed by XPS and EDXS measurements, occurred in an amorphous phase. Moreover, the gold crystallite average size (evaluated using the Scherrer equation on the XRD diffractograms) was about 20 nm, increasing to 40 nm upon prolonged irradiation time in the case of T100 samples, whereas in the case of SDS ones, the average size was practically unchanged upon increased irradiation. The back-scattered SEM and TEM microscopies used to get information about the nanocomposite morphology revealed that gold NPs are uniformly distributed on the oxide surface. Furthermore, XPS outcomes, besides confirming the formation of both metallic gold and titania, also provided information about the wide dispersion of Au NPs on the TiO_2 surface. In fact, the Au : Ti ratio (1.5) was much higher than the stoichiometric one (0.25).

The thorough investigations carried out outlined that the properties of the final system (gold particle sizes and distribution) are strongly dependent on the choice of miniemulsion system and irradiation time. The miniemulsion system based on the non-ionic surfactant Triton X-100 is less favourable to form small gold particles at long irradiation time, which instead favours their growth. In contrast, SDS-based miniemulsion systems favour the formation of small sized gold particles of maximum 25 nm at any irradiation time. In both cases gold particles are finely dispersed on the supporting titania matrix, as confirmed by TEM and SEM. Our results from XPS clearly show that a high degradation of precursor material up to 88% can be induced by variation of the irradiation time.

In addition, the SDS-8 materials obtained were tested as catalysts for the oxidation of 2-propanol, showing increased catalytic activity, compared to the Au/TiO_2 reference obtained by UV decomposition of the precursor in aqueous solution.

In conclusion, it was shown that using a combined miniemulsion/single-source precursor approach, the formation of Au/TiO_2 nanocomposites with crystalline Au NPs on amorphous TiO_2 could be afforded, and that the obtained nanocomposite has also appreciable catalytic activity in model oxidation reactions.

Experimental

Materials

All chemicals were used without further purification. Sodium dodecylsulfate (SDS, $NaC_{12}H_{25}SO_4$), Triton X-100, (octylphenylether, $(C_{14}H_{22}O(C_2H_4O)_n$, $n = 9$–$10)$), ethanol (C_2H_5OH), 1-pentanol ($C_5H_{11}OH$), and *n*-heptane (C_7H_{16}) were purchased from Aldrich (Milan, Italy). All chemicals were used without further purification.

Synthesis of the single-source precursor $AuCl_4(NH_4)_7[Ti_4(O_2)_4(Hcit)_2(cit)_2] \cdot 12H_2O$

The precursor $AuCl_4(NH_4)_7[Ti4(O_2)_4(Hcit)_2(cit)_2] \cdot 12H_2O$ was synthesized as reported elsewhere.[6] See Fig. SI-19 in the ESI† for the Raman spectrum, confirming the presence of the Ti-peroxide group.

Preparation of Au/TiO_2 nanocomposites in a miniemulsion with ionic surfactant SDS

In a typical synthesis, 160 mg (9.2×10^{-5} mol) of the precursor were dispersed in water (10 ml), and this aqueous suspension was then added under mechanical stirring to a surfactant–solvent mixture (5.0 g SDS, 10.0 g pentanol and 25.0 g heptane;

1/2/5 w/w ratio). The resulting emulsion was then sonicated for 3 minutes (using a Sartorius Stedim Labsonic P sonifier), with an acoustic power of 322 W cm^{-2}, to generate a miniemulsion, and subsequently irradiated with a UV lamp (125 W) for 4 and 8 hours. After this treatment, the suspension turned from bright yellow to dark purple. The solid obtained was recovered by centrifugation (7000 rpm for 5 minutes) and washed with ethanol and water.

Preparation of Au/TiO_2 nanocomposites in a miniemulsion with non-ionic surfactant Triton X-100

In a typical synthesis, 152 mg (8.7×10^{-5} mol) of the precursor were dispersed in water (4 ml), and this aqueous suspension was then added under mechanical stirring to a surfactant–solvent mixture (6 g Triton X-100, 1.62 g pentanol and 46.8 g cyclohexane; 3/1/23 w/w ratio). The resulting emulsion was then sonicated for 3 minutes, with an acoustic power of 322 W cm^{-2}, to generate a miniemulsion, and subsequently irradiated with a UV lamp for 4 and 8 hours. After this treatment, the suspension turned from bright yellow to dark purple. The solid obtained was recovered by centrifugation (7000 rpm for 5 minutes) and washed with ethanol and water.

Catalytic testing

Prior to catalytic testing the samples were calcined for two hours at 600 °C. Therefore 250 mg of the Au/TiO_2 powder were dispersed in a quartz crucible and placed in a tube furnace at an airflow of 20 ml min^{-1}, and heated at 5 K min^{-1}. Gaseous phase oxidation of 2-propanol was performed in a vertical, fixed bed reactor filled with 75 mg of the sample on glass wool. Oxidation experiments were carried out for 3 h at 140 °C (413 K) with a 2-propanol/oxygen ratio of 1 : 2 mol mol^{-1}, at a total gas flow of 18 ml min^{-1}. 2-Propanol was therefore provided by a saturated nitrogen flow. Condensable reaction products were collected in a cold trap (243 K), and CO and CO_2 were analyzed with a gas detector. Liquid phase oxidation of 2-propanol (5% aq. solution) was performed in a commercial high pressure reactor BR-40 from Berghof, equipped with a thermal sensor connected to an automatic heating control, liquid sample extraction valve, gas feeding, inert inlets (TFPE) and a stirring bar. The experiments were conducted at an initial pressure of 7 atm, in synthetic air, 750 rpm stirring velocity, and 5 K min^{-1} heat ramp, up to 120 °C (393 K), holding the temperature for 2.5 h. Afterwards the heating was removed and the reactor was cooled to room temperature without further stirring. All liquid samples were analyzed by GC, using an Agilent 7820A equipped with DB-5 (30 m, 0.32 diameter, 1 μm film) and DB-WAX (30 m, 0.32 diameter, 0.5 μm film) columns.

Characterization

XPS was carried out with a Perkin-Elmer Φ 5600ci instrument using standard Al-K_α radiation (1486.6 eV) operating at 350 W. The working pressure was $<5 \times 10^{-8}$ Pa. The calibration was based on the binding energy (BE) of the $Au4f_{7/2}$ line at 83.9 eV with respect to the Fermi level. The standard deviation for the BE values was 0.15 eV. The reported BEs were corrected for the BE charging effects, assigning the BE value of 284.6 eV to the C1s line of carbon. Survey scans were obtained in the 0–1350 eV range (pass energy 187.5 eV, 1.0 eV per step, 25 ms per step). Detailed scans (58.7 eV pass energy, 0.1 eV per step, 50–150 ms per step) were recorded for the O1s, C1s, Au4f, Au4d, Ti2p, TiLMM, N1s and Na1s regions. The atomic composition, after a Shirley-type background subtraction,[43] was evaluated using sensitivity factors supplied by Perkin-Elmer.[37] Charge effects were partially compensated using a charge neutralizer (flood gun). Peak assignment was carried out according to literature data.[37] The thermogravimetric analyses (TGA) were performed in air on a LabSys Setarm SDT 2960 instrument in the temperature range 20–800 °C using a heating rate of 10 °C min^{-1}. The XRD data were collected with a Bruker D8 Advance Diffractometer equipped with a Göbel mirror. The angular accuracy was 0.001° and the angular resolution was better than 0.01°. The average crystallite sizes were calculated by means of the Scherrer formula from the most intense peaks of each spectrum. Further wide angle X-ray diffraction patterns were recorded using a Philips X'Pert PRO diffractometer operating in the θ–2θ geometry, equipped with a graphite monochromator on the diffracted beam (CuK_α radiation). For transmission electron microscopy (TEM) analyses two different instrumentations were used. Higher resolution images were acquired using a Hitachi H-8100 electron microscope (accelerating voltage of up to 200 kV, LaB_6 filament). For general images and selected area electron diffraction (SAED) patterns, a Philips CM12 microscope, operating at a maximum voltage of 120 kV, was used. Both microscopes were equipped with an energy dispersive X-ray spectroscopy (EDXS) apparatus, used to measure qualitatively the composition of the observed sample regions. SAED patterns were indexed with the software package Process Diffraction.[44] Sample preparation was quite straightforward, as it required spreading a drop of a sonicated alcohol suspension of the powder samples on a carbon coated copper TEM grid. The microstructure of the Au/TiO_2 nanocomposites (precipitates obtained before heating the suspensions at 80 °C were also investigated) was analyzed using scanning electron microscopy (SEM). Measurements were performed using a field emission SEM, Zeiss SUPRA 35VP, that, as TEMs, was equipped with an EDXS system (Oxford INCA).

Acknowledgements

Dr Chiara Maccato (Dipartimento di Scienze Chimiche, Università di Padova) is gratefully acknowledged for SEM measurements and helpful discussion.

Notes and references

1 M. Valden, X. Lai and D. W. Goodman, *Science*, 1998, **281**, 1647.
2 J. Zhao, S. Sallard, B. M. Smarsly, S. Gross, M. Bertino, C. Boissiere, H. Chen and J. Shi, *J. Mater. Chem.*, 2010, **20**, 2831.
3 X. Wang, D. R. G. Mitchell, K. Prince, A. J. Atanacio and R. A. Caruso, *Chem. Mater.*, 2008, **20**, 3917.

4 H. Li, Z. Bian, J. Zhu, Y. Huo, H. Li and Y. Lu, *J. Am. Chem. Soc.*, 2007, **129**, 4538.
5 L. Armelao, D. Barreca, G. Bottaro, A. Gasparotto, E. Tondello, M. Ferroni and S. Polizzi, *Chem. Mater.*, 2004, **16**, 3331.
6 M. Rohe, E. Loeffler, M. Muhler, A. Birkner, C. Woell and K. Merz, *Dalton Trans.*, 2008, 6106.
7 J. S. Ratliff, S. A. Tenney, X. Hu, S. F. Conner, S. Ma and D. A. Chen, *Langmuir*, 2009, **25**, 216.
8 N. Chandrasekharan and P. V. Kamat, *J. Phys. Chem. B*, 2000, **104**, 10851.
9 A. Vittadini and A. Selloni, *J. Chem. Phys.*, 2002, **117**, 353.
10 C. H. Tseng, T. C. K. Yang, H. E. Wu and H. C. Chiang, *J. Hazard. Mater.*, 2009, **166**, 686.
11 N. Zheng and G. D. Stucky, *Chem. Commun.*, 2007, 3862.
12 J. D. Grunwaldt and A. Baiker, *J. Phys. Chem. B*, 1999, **103**, 1002.
13 A. Karpenko, Y. Denkwitz, V. Plzak, J. Cai, R. Leppelt, B. Schumacher and R. J. Behm, *Catal. Lett.*, 2007, **116**, 105.
14 J. Leerat, S. Osuwan and E. Gulari, *Catal. Lett.*, 2011, **141**(1), 62.
15 S. Zhao, G. Ramakrishnan, D. Su, R. Rieger, A. Koller and A. Orlov, *Appl. Catal., B*, 2011, **104**, 239.
16 A. Orlov, D. A. Jefferson, N. Macleod and M. Lambert, *Catal. Lett.*, 2004, **92**, 41.
17 Y. Takahashi and T. Tatsuma, *Appl. Phys. Lett.*, 2011, **99**, 182110.
18 M. Antonietti, *Colloid Chemistry II*, Springer, Berlin/Heidelberg, 2003.
19 K. Landfester, *Adv. Mater.*, 2001, **13**, 765.
20 K. Landfester, *Annu. Rev. Mater. Res.*, 2006, **36**, 231.
21 M. Antonietti and K. Landfester, *Prog. Polym. Sci.*, 2002, **27**, 689.
22 K. Landfester and M. Antonietti, in *Colloids and Colloid Assemblies*, Wiley-VCH, Weinheim, Germany, 2004, ch. 6, p. 175.
23 R. Rossmanith, C. K. Weiss, J. Geserick, N. Hüsing, U. Hoermann, U. Kaiser and K. Landfester, *Chem. Mater.*, 2008, **20**, 5768.
24 R. Schiller, C. K. Weiss, J. Geserick, N. Hüsing and K. Landfester, *Chem. Mater.*, 2009, **21**, 5088.
25 R. Muñoz-Espi, K. C. Weiss and K. Landfester, *Curr. Opin. Colloid Interface Sci.*, 2012, **17**, 212–224.
26 T. N. Vorobyova, O. N. Vrublevskaya and A. V. Vengura, *Surf. Coat. Technol.*, 2005, **200**, 2481.
27 K. Tomita, V. Petrykin, M. Kobayashi, M. Shiro, M. Yoshimura and M. Kakihana, *Angew. Chem.*, 2006, **118**, 2438–2441; *Angew. Chem., Int. Ed.*, 2006, **45**, 2378–2381.
28 Y. F. Deng, Z. H. Zhou, H. L. Wan and K. R. Tsai, *Inorg. Chem. Commun.*, 2004, **7**, 169.
29 M. P. Seah, G. C. Smith and M. T. Anthony, *Surf. Interface Anal.*, 1990, **15**, 293.
30 M. T. Anthony and M. P. Seah, *Surf. Interface Anal.*, 1984, **6**, 95.
31 G. Johansson, J. Hedman, A. Berndtsson, M. Klasson and R. Nilsson, *J. Electron Spectrosc. Relat. Phenom.*, 1973, **2**, 295.
32 W. McLean, C. A. Colmenares, R. L. Smith and G. Somorjai, *J. Phys. Chem.*, 1983, **87**, 788.
33 J. Yu, J. Xiong, B. Cheng and S. Liu, *Appl. Catal., B*, 2005, **60**, 211.
34 H. E. Chao, Y. U. Yun, H. U. Xingfang and A. Larbot, *J. Eur. Ceram. Soc.*, 2003, **23**, 1457.
35 C. He, Y. Yu, X. Hu and A. Larbot, *Appl. Surf. Sci.*, 2002, **200**, 239.
36 L. Armelao, D. Barreca, G. Bottaro, A. Gasparotto, S. Gross, C. Maragno and E. Tondello, *Coord. Chem. Rev.*, 2006, **250**, 1294.
37 W. F. Stickle, J. F. Moulder, P. E. Sobol and K. D. Bomben, *Handbook of X-ray Photoelectron Spectroscopy*, Perkin-Elmer, Eden Prairie, MN, 1992.
38 S. O. Saied, J. L. Sullivan, T. Choudhury and C. G. Pearce, *Vacuum*, 1988, **38**, 917.
39 W. E. Slinkard and P. D. DeGroot, *J. Catal.*, 1981, **68**, 423.
40 G. M. Ingo, S. Dirè and F. Babonneau, *Appl. Surf. Sci.*, 1993, **70–71**, 230.
41 J. A. Mejias, V. M. Jimenez, G. Lassaletta, A. Fernandez, J. P. Espinos and A. R. Gonzalez-Elipe, *J. Phys. Chem.*, 1996, **100**, 16255.
42 A. Fernandez, A. Caballero, A. R. Gonzalez-Elipe, J. M. Herrmann, H. Dexpert and F. Villain, *J. Phys. Chem.*, 1995, **99**, 3303.
43 D. A. Shirley, *Phys. Rev. B: Solid State*, 1972, **5**, 4709.
44 L. Labar Janos, *Ultramicroscopy*, 2005, **103**, 237.